

# Optical deflection and sorting of microparticles in a near-field optical geometry

R. F. Marchington<sup>1\*</sup>, M. Mazilu<sup>1</sup>, S. Kuriakose<sup>2</sup>, V. Garcés-Chávez<sup>1</sup>, P. J. Reece<sup>1</sup>,  
T. F. Krauss<sup>1</sup>, M. Gu<sup>2</sup>, and K. Dholakia<sup>1</sup>

<sup>1</sup> SUPA, School of Physics and Astronomy, University of St. Andrews,  
North Haugh, St. Andrews, KY16 9SS, Scotland, UK

<sup>2</sup> Centre for Micro-Photonics, Faculty of Engineering and Industrial Sciences,  
Swinburne University of Technology, Hawthorn, VIC- 3122, Australia

\*Corresponding author: [rm346@st-andrews.ac.uk](mailto:rm346@st-andrews.ac.uk)

**Abstract:** Near-field optical micromanipulation permits new possibilities for controlled motion of trapped objects. In this work, we report an original geometry for optically deflecting and sorting micro-objects employing a total internal reflection microscope system. A small beam of laser light is delivered off-axis through a total internal reflection objective which creates an elongated evanescent illumination of light at a glass/water interface. Asymmetrical gradient and scattering forces from this light field are seen to deflect and sort polystyrene microparticles within a fluid flow. The speed of the deflected objects is dependent upon their intrinsic properties. We present a finite element method to calculate the optical forces for the evanescent waves. The numerical simulations are in good qualitative agreement with the experimental observations and elucidate features of the particle trajectory. In the size range of 1  $\mu\text{m}$  to 5  $\mu\text{m}$  in diameter, polystyrene spheres were found to be guided on average  $2.9 \pm 0.7$  faster than silica spheres. The velocity increased by  $3.0 \pm 0.5 \mu\text{ms}^{-1}$  per  $\mu\text{m}$  increase in diameter for polystyrene spheres and  $0.7 \pm 0.2 \mu\text{ms}^{-1}$  per  $\mu\text{m}$  for silica. We employ this size dependence for performing passive optical sorting within a microfluidic chip and is demonstrated in the accompanying video.

©2008 Optical Society of America

**OCIS codes:** (180.4243) Near-field microscopy; (240.6690) Surface waves; (260.6970) Total internal reflection; (350.4855) Optical tweezers or optical manipulation;

---

## References and links

1. M. Gu, J. B. Haumonte, Y. Micheau, J. W. M. Chon, and X. S. Gan, "Laser trapping and manipulation under focused evanescent wave illumination," *Appl. Phys. Lett.* **84**, 4236-4238 (2004).
2. V. Garcés-Chávez, K. Dholakia, and G. C. Spalding, "Extended-area optically induced organization of microparticles on a surface," *Appl. Phys. Lett.* **86**, 031106 (2005).
3. V. Garcés-Chávez, R. Quidant, P. J. Reece, G. Badenes, L. Torner, and K. Dholakia, "Extended organization of colloidal microparticles by surface plasmon polariton excitation," *Phys. Rev. B* **73**, 085417 (2006).
4. P. J. Reece, V. Garcés-Chávez, and K. Dholakia, "Near-field optical micromanipulation with cavity enhanced evanescent waves," *Appl. Phys. Lett.* **88**, 221116 (2006).
5. S. Kawata and T. Tani, "Optically driven mie particles in an evanescent field along a channeled waveguide," *Opt. Lett.* **21**, 1768-1770 (1996).
6. K. Dholakia, W. M. Lee, L. Paterson, M. P. MacDonald, R. McDonald, I. Andreev, P. Mthunzi, C. T. A. Brown, R. F. Marchington, and A. C. Riches, "Optical separation of cells on potential energy landscapes: Enhancement with dielectric tagging," *IEEE J. Sel. Top. Quantum. Electron.* **13**, 1646-1654 (2007).
7. M. P. MacDonald, G. C. Spalding, and K. Dholakia, "Microfluidic sorting in an optical lattice," *Nature* **426**, 421-424 (2003).
8. K. Ladavac, K. Kasza, and D. G. Grier, "Sorting mesoscopic objects with periodic potential landscapes: Optical fractionation," *Phys. Rev. E* **70**, 010901 (2004).
9. G. Milne, D. Rhodes, M. MacDonald, and K. Dholakia, "Fractionation of polydisperse colloid with acousto-optically generated potential energy landscapes," *Opt. Lett.* **32**, 1144-1146 (2007).

10. L. Paterson, E. Papagiakoumou, G. Milne, V. Garcés-Chávez, S. A. Tatarkova, W. Sibbett, F. J. Gunn-Moore, P. E. Bryant, A. C. Riches, and K. Dholakia, "Light-induced cell separation in a tailored optical landscape," *Appl. Phys. Lett.* **87**, 123901 (2005).
11. I. Ricardez-Vargas, P. Rodríguez-Montero, R. Ramos-García, and K. Volke-Sepulveda, "Modulated optical sieve for sorting of polydisperse microparticles," *Appl. Phys. Lett.* **88**, 121116 (2006).
12. T. Čižmár, M. Šiler, M. Šerý, P. Zemánek, V. Garcés-Chávez, and K. Dholakia, "Optical sorting and detection of submicrometer objects in a motional standing wave," *Phys. Rev. B* **74**, 035105 (2006).
13. K. Grujic, O. G. Helleso, J. P. Hole, and J. S. Wilkinson, "Sorting of polystyrene microspheres using a y-branched optical waveguide," *Opt. Express* **13**, 1-7 (2005).
14. B. S. Schmidt, A. H. J. Yang, D. Erickson, and M. Lipson, "Optofluidic trapping and transport on solid core waveguides within a microfluidic device," *Opt. Express* **15**, 14322-14334 (2007).
15. D. Ganic, X. S. Gan, and M. Gu, "Trapping force and optical lifting under focused evanescent wave illumination," *Opt. Express* **12**, 5533-5538 (2004).
16. R. J. Oetama, and J. Y. Walz, "Translation of colloidal particles next to a flat plate using evanescent waves," *Colloids Surf. A* **211**, 179-195 (2002).
17. J. P. Barton, and D. R. Alexander, "Fifth-order corrected electromagnetic field components for a fundamental gaussian beam," *J. Appl. Phys.* **66**, 2800-2802 (1989).
18. I. Brevik, "Experiments in phenomenological electrodynamics and the electromagnetic energy-momentum tensor," *Phys. Rep.* **52**, 133-201 (1979).
19. J. P. Barton, D. R. Alexander, and S. A. Schaub, "Theoretical determination of net radiation force and torque for a spherical particle illuminated by a focused laser beam," *J. Appl. Phys.* **66**, 4594-4602 (1989).
20. E. Almaas, and I. Brevik, "Radiation forces on a micrometer-sized sphere in an evanescent field," *J. Opt. Soc. Am. B* **12**, 2429-2438 (1995).
21. A. J. Goldman, R. G. Cox, and H. Brenner, "Slow viscous motion of a sphere parallel to a plane wall. I. Motion through a quiescent fluid," *Chem. Eng. Sci.* **22**, 637-651 (1967).
22. A. H. J. Yang and D. Erickson, "Stability analysis of optofluidic transport on solid-core waveguiding structures," *Nanotechnology* **4**, 045704 (2008).
23. G. P. Krishnan and D. T. Leighton, "Inertial lift on a moving sphere in contact with a plane wall in a shear-flow," *Phys. Fluids* **7**, 2538-2545 (1995).
24. I. Brevik, T. A. Sivertsen, and E. Almaas, "Radiation forces on an absorbing micrometer-sized sphere in an evanescent field," *J. Opt. Soc. Am. B* **20**, 1739-1749 (2003).
25. F. Charru, E. Larrieu, J. B. Dupont, and R. Zenit, "Motion of a particle near a rough wall in a viscous shear flow," *J. Fluid Mech.* **570**, 431-453 (2007).
26. J. C. McDonald and G. M. Whitesides, "Poly(dimethylsiloxane) as a material for fabricating microfluidic devices," *Acc. Chem. Res.* **35**, 491-499 (2002).
27. S. B. Kim, J. H. Kim, and S. S. Kim, "Theoretical development of in situ optical particle separator: Cross-type optical chromatography," *Appl. Opt.* **45**, 6919-6924 (2006).
28. G. Milne, "Labview pattern-matching particle tracker software," (2007), <http://faculty.washington.edu/gmilne/tracker.htm>.
29. M. Šiler, T. Čižmár, M. Šerý, and P. Zemánek, "Optical forces generated by evanescent standing waves and their usage for sub-micron particle delivery," *Appl. Phys. B* **84**, 157-165 (2006).
30. S. J. Hart and A. V. Terray, "Refractive-index-driven separation of colloidal polymer particles using optical chromatography," *Appl. Phys. Lett.* **83**, 5316-5318 (2003).

## 1. Introduction

Near-field optical micromanipulation has come to the research forefront in recent years with the promise of powerful trapping geometries, localization of objects close to an interface and the prospect of large scale area patterning of colloidal particles. Trapping of microparticles has been shown using a total internal reflection (TIR) microscope objective that has been illuminated with an annular beam [1]. In the Kretschmann geometry, prisms have been used to optically organize more than a thousand microparticles, in an extended area, to form large scale particle arrays [2]. Techniques such as surface plasmons [3] and optical cavities [4] have been employed for near-field enhancement. It has been demonstrated that optical forces arising from an evanescent field can be strong enough to hold a single microparticle at the interface of two media of different refractive indices (for example, glass/water) [1]. Scattering forces in the near-field have also been used for propelling microparticles atop a waveguide [5].

The ability not solely to trap but indeed to separate or sort microscopic particles and cells is a topic of current interest within the broader field of optical micromanipulation [6]. To achieve such a goal in a passive manner is appealing as it obviates the need to add any

dielectric tags or surface markers (e.g. fluorophores). Thus much interest has been focused on the potential of passive sorting techniques in recent years. Optical separation of objects has previously been shown with and without the inclusion of a fluid flow. In particular, studies have shown the deflection of objects on optical potential energy landscapes in the presence of a fluid flow, where the Stokes forces from the fluid flow complements the optical forces. The optical forces are critically dependent upon the intrinsic characteristics (e.g. size, refractive index) of the object causing a selective angular deflection of objects. Studies have been performed with interference patterns (optical potential energy landscapes) [7], holographic methods [8] and acousto-optic techniques [9]. Interesting dynamics as well as fractionation capabilities have been observed. Separate studies have also explored the motion and sorting of microparticles and red/white blood cells in the absence of a fluid flow [10-12]. Interestingly, this latter study by Cizmar, *et al.*, demonstrated the potential use of near-field optical standing waves for delivery and sorting of microparticles in a tilted washboard potential, though this was as stated with no fluid flow present. Separately, sorting of objects has been seen in an active manner upon a waveguide, that involves the switching of the light fields between ports by the user [13]. Another study characterizes the size dependence of the optical guiding force of particles atop a waveguide in the presence of fluid flow [14].

In this paper, we study experimentally and theoretically the optical deflection and passive sorting of micro-objects in a reconfigurable near-field geometry. Our system consists of an off-axis collimated laser beam (which we term for simplicity as a “beamlet”) of small diameter that is focused with a TIR objective at an interface between two media of different refractive indices, creating an elliptical beam focus at the interface. We consider micron-sized particles over the projected evanescent field and determine the optical forces, the trajectories and velocity of the particles. We show that these depend on their size, refractive index, the incident laser power and its state of polarization.

More precisely, in this paper we explore the following theoretical and experimental aspects of evanescent field sorting:

- (i) Theoretically, we review the optical force calculation based on the Maxwell stress tensor formalism and its associated force density. The microfluidic effects are treated using wall corrected Stokes drag coefficient and we compare the hydrodynamic velocities obtained when the particles are in contact with the substrate or when further away. The numerical simulation uses a fully vectorial finite element method which is validated against existing literature.
- (ii) Experimentally, we verify the near-field deflection force for our new TIR geometry and find it to be in qualitative agreement with our theoretical calculations. The dependence of the evanescent deflection force on particle size and refractive index is investigated and we progress to initiate passive optical sorting of microparticles in a microfluidic chip.

This work is in contrast to the work in [1] where an annular beam was used to instigate trapping through a TIR objective, with the beam geometry resulting in cancellation of any scattering forces parallel to the interface. Depending upon the position and input angle of the beamlet we may induce an evanescent field, a combination of evanescent and transmitted fields or solely transmitted light at the interface. The interplay of gradient and scattering forces create unbalanced or deflective forces nearby the focal plane close to the surface. In an evanescent wave geometry, microparticles are attracted to the surface due to gradient forces [15] and subsequently may be guided by the optical field in the direction of evanescent wave propagation [16] due to the induced scattering forces. These scattering forces indeed may be balanced to create large area near-field trapping [2].

In Section 2, we briefly review the theory and numerical model that underpins our experimental observations, which are described in Section 3.

## 2. Theoretical model

### 2.1 Optical configuration, beam properties and Maxwell's stress tensor

The inset in Fig. 1 shows the optical configuration of our experiment together with the electric field of the beam undergoing total internally reflected (TIR) on the glass-water interface (in red). The sphere, depicted in blue, shows the overlap between the non-disturbed electric field and the particles. This non-disturbed field decays exponentially above the substrate. For the numerical simulations we have considered the non-absorbing dielectric case where all the indices of refraction are real, with  $n=1.33$  for water,  $n=1.59$  for the polystyrene particle and  $n=1.515$  for the substrate. Using these parameters, Fig. 1 shows the penetration depth,  $z_p$ , of the TIR beam as a function of the angle of incidence, as defined by  $z_p = 1/\text{Im}(k_{z1})$  where  $k_{z1}$  is the complex wavevector in water in the direction perpendicular to the substrate. This penetration depth is infinite for propagating waves whose angle of incidence are below the critical angle (here  $61.4^\circ$ ). Above the critical angle the penetration depth decreases as the angle increases. Consequently the overlap and the optical forces decrease as this angle increases.

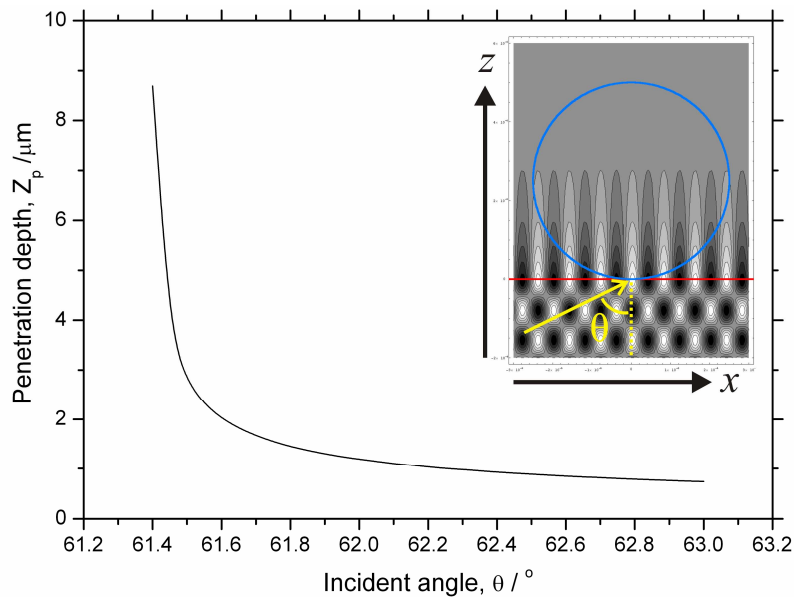


Fig. 1. Penetration depth of the evanescent wave as a function of the incidence angle at the interface. The inset shows the overlap between the evanescent field and the particle at the interface between the substrate and the water (angle of incidence,  $\theta = 62^\circ$  and a  $5 \mu\text{m}$  sphere). The interaction between sphere and field is not considered in this illustration.

The beam that we consider in our simulation is a fully vectorial linearly polarized Gaussian beam in the first order of development [17]. By capturing the back reflection of the beam, as the height of the water-glass interface is changed, we estimate the angle of incidence to be approximately  $61^\circ$ , as depicted in Fig. 2. Unfortunately, due to optical distortions and multiple reflections the intensity profile has lost its perfect Gaussian shape. We further decompose this Gaussian beam in a minimal set of plane waves for which we calculate analytically the complex transmission and reflection coefficients at the water-glass interface. The superposition of these plane waves enables us to treat analytically a single incident field that includes the incoming, the reflected and the evanescent parts. Further, these waves form a minimal angular spectral decomposition of the incoming beam and the unit angle between two

plane waves, within this spread, is given by the far-field divergence angle of the Gaussian beam.

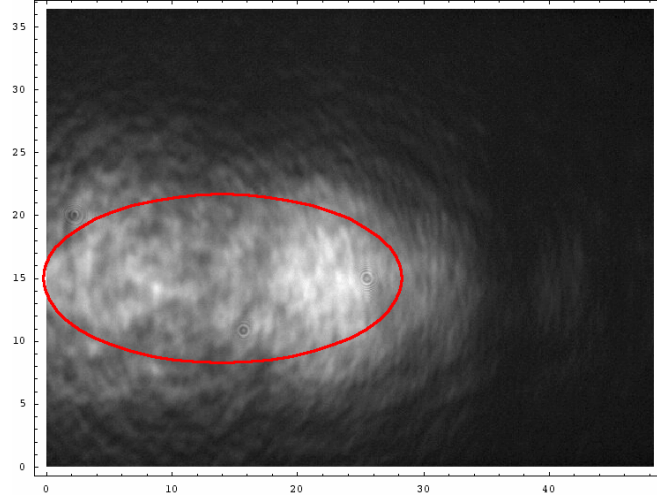


Fig. 2. Comparison between the experimentally observed beam profile and the beam waist (in red) of a Gaussian beam incident at  $61^\circ$ . The units on the  $x$ - and  $y$ -axis are  $\mu\text{m}$  and in normal incidence the Gaussian beam has a diameter of  $13.4 \mu\text{m}$ .

We calculate the total optical force acting on a particle by integrating the Maxwell's stress tensor on the surface of the particle. In a host material the stress-tensor  $\overline{\overline{T}}$  is given by [18,19]

$$\overline{\overline{T}} = \overline{\overline{D}} \otimes \overline{\overline{E}}^* + \overline{\overline{B}} \otimes \overline{\overline{H}}^* - \frac{1}{2}(\overline{\overline{D}} \bullet \overline{\overline{E}}^* + \overline{\overline{B}} \bullet \overline{\overline{H}}^*), \quad (1)$$

with  $\overline{\overline{E}}$ ,  $\overline{\overline{D}}$ ,  $\overline{\overline{H}}$  and  $\overline{\overline{B}}$  denoting the electric field, the electric displacement, the magnetic field and magnetic flux respectively. Applying the constitutive relations  $\overline{\overline{D}} = \epsilon_r \epsilon_0 \overline{\overline{E}}$  and  $\overline{\overline{B}} = \mu_r \mu_0 \overline{\overline{H}}$ , where  $\epsilon_r$ ,  $\epsilon_0$ ,  $\mu_r$  and  $\mu_0$  are the relative and vacuum permittivity and permeability respectively, we find in SI units

$$T_{ij} = \epsilon_r \epsilon_0 E_i E_j^* + \mu_r \mu_0 H_i H_j^* - \frac{1}{2}(\epsilon_r \epsilon_0 E_k E_k^* + \mu_r \mu_0 H_k H_k^*), \quad (2)$$

where we sum over the identical indices  $k$ . The optical average force acting on the particle is

$$\langle \overline{\overline{F}} \rangle = \frac{1}{2} \text{Re} \left( \int_s \overline{\overline{T}} \bullet \overline{\overline{n}} ds \right), \quad (3)$$

where  $\overline{\overline{n}}$  is the normal vector pointing outward to the surface  $S$  of the particle. Here, we average over one optical cycle. Note that, due to the jump in the index of refraction, the normal fields at the surface of the particles have a discontinuity. To calculate the total optical force we use the external fields. In this case, the total force includes not only the optical force on the particle but also the optical force acting on the water interface, which is completely transmitted, to the sphere because of the hydrodynamic non-slip boundary conditions at this interface.

To validate the integrated stress tensor approach, we compare it with the integrated force density

$$\langle \vec{F} \rangle = -\frac{\epsilon_0}{4} \text{Re} \left( \int_V E_k^* E_k \nabla \epsilon_r dv \right) \quad (4)$$

where the integral is taken over the volume of the particle [18]. The permittivity,  $\epsilon_r$ , is constant in the volume of the particle, hence the integrand is only non-zero on the surface of the sphere and the above integral simplifies to a surface integral. Even though analytically both force calculation methods should give identical results, we observe that this is only the case when the numerical discretization of the problem has sufficient resolution. This important consideration allows us to verify the validity of our numerical simulation.

### 2.3 Numerical simulation

We used a finite element method program *Comsol* to calculate the scattered electric and magnetic fields. For simplicity, we assumed negligible power loss when propagating through the optical system. Additionally, we assume the water-glass interface to correspond to the focal plane of the Gaussian beam. Throughout the paper, the  $p$ -polarized evanescent field is defined as parallel to the plane of incidence and  $s$ -polarized as perpendicular.

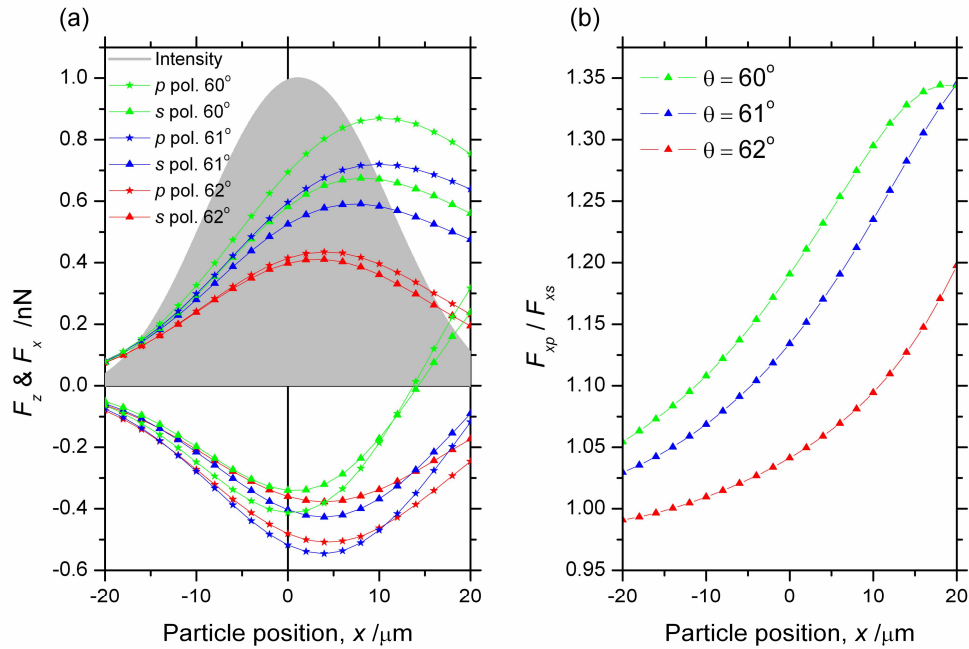


Fig. 3. (a). Horizontal (positive range) and vertical (negative range) forces as a function of the particle position with respect to the incoming beam, for different angles of incidence. The grayed region corresponds to the intensity profile of the beam on the interface. Note that its maximum is shifted with respect to the center of the incident beam due to the Goos-Hänchen shift. (b) Ratio between the horizontal optical forces of the  $p$  and  $s$  polarizations as a function of the particle position for different angles of incidence.

To test robustness of the numerical model, we have simulated the same illustrative example as Almaas and Brevik [20], corresponding to a  $2 \mu\text{m}$  glass sphere ( $n = 1.5$ ) submerged in water ( $n = 1.33$ ) above a substrate ( $n = 1.75$ ) having a higher index of refraction. In this configuration, the critical angle is  $51^\circ$  and the beam has a power of  $150 \text{ mW}$  and a  $100 \mu\text{m}$  diameter. This corresponds to a power density of  $19 \text{ MWm}^{-2}$  and a force coefficient of  $\epsilon_0 E^2 a^2 = 130 \text{ fN}$  where  $a$  is the radius of the particle. Using these same parameters our model predicts horizontal guiding forces of  $F_{xp} = 11 \text{ fN}$  for  $p$ -polarization and  $F_{xs} = 8.1 \text{ fN}$  for  $s$ -polarization, which compare respectively to  $10 \text{ fN}$  and  $8.1 \text{ fN}$  [20].

Similarly, our calculation imply we pull the particle towards the substrate with  $F_{zp} = -44$  fN ( $p$ -pol.) and  $F_{zs} = -27$  fN ( $s$ -pol.) which is in good agreement with  $-44$  fN and  $-29$  fN presented in reference [20].

Figure 3 shows the main result of our simulation i.e. the horizontal and vertical optical forces acting on the particle at different positions along the middle of the TIR beam profile. The considered particle is  $5\ \mu\text{m}$  in diameter and is in contact with the substrate. The  $1\ \text{W}$  optical power of the beam with a spot size of  $13.4\ \mu\text{m}$  leads to a power density of  $10\ \text{GWm}^{-2}$ , while the force coefficient  $\epsilon_0 E^2 a^2 = 420\ \text{pN}$  is three thousand times larger than the previous test case. The positive part of the graph shows the horizontal, i.e. guiding forces, while the negative part shows the vertical forces, i.e. the pull/push towards the substrate. The grayed region shows intensity of the TIR beam together with the Goos-Hänchen shift. Further, depending on the angle of incidence, position in the beam and distance from the substrate, we observe a variable ratio between the  $s$  and  $p$  polarizations [see Fig. 3(b)]. First of all, using this graph, we can observe a clear shift between the maximum beam intensity and the maximum force amplitude. This shift, similar to the Goos-Hänchen shift but more pronounced, starts before the critical angle and decreases for angles far beyond the critical angle. Further point that we note is the difference in the pull force profile between the propagating case (green curve) and the evanescent cases (red and blue curves). Indeed, when the beam is mostly propagating, we can observe an inversion of the vertical force, which at first is pulling and later pushing the particle away from the interface.

The difference in force magnitudes as a function of angle can also be observed in Fig. 4 where we have displayed the vertical and horizontal forces in the center of the incident beam as a function of the angle of incidence. Just like in Fig. 3, we see that close to the critical angle the propagating beams still attract the particles towards the water glass interface while guiding it very efficiently. In this case the particle acts like a small micro-lens that bends the light away from the interface [see field distribution in Fig. 4(b)]. This, in turn, pulls the particle towards the interface, due to momentum conservation.

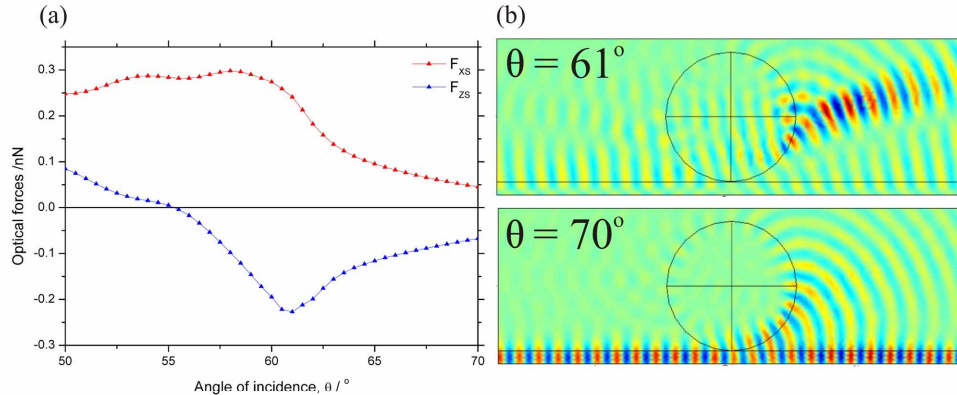


Fig. 4. (a). Horizontal and vertical forces as a function of the angle of incidence for a  $5\ \mu\text{m}$  particles and an  $s$  polarized beam. b) Electric field distribution for  $61^\circ$  and  $70^\circ$  (see supplementary video)

Most importantly, for our sorting application (described later), we determined the guiding forces to depend linearly on the size of the particles (see Fig. 5). This linear relationship has its origin in the relatively large particles considered here and the small refractive index difference between the water, the particle and the substrate. Indeed, for high contrast small particles we expect a complex relationship between guiding forces and particle size [20].

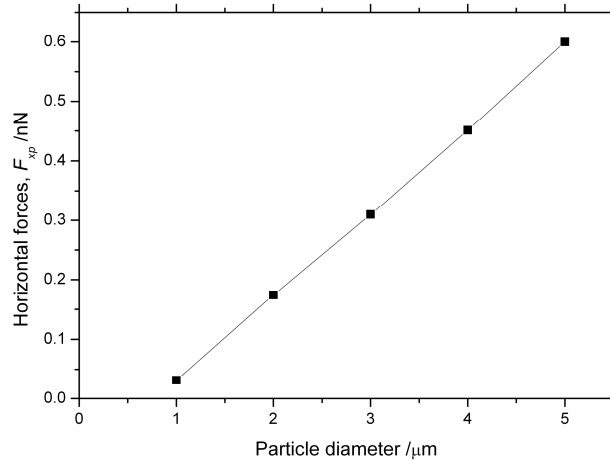


Fig. 5. Linear dependence of the horizontal forces for  $p$  polarized centered beam at  $x = 0$  incident at  $\theta = 61^\circ$  as a function of the particle diameter.

### 2.3 Microfluidic effects; colloidal dynamics near a wall

When guided by the evanescent field, the particle moves along a planar substrate. In this case, the standard bulk Stokes drag coefficient  $F = 6\pi\mu av$ , where  $\mu$  is the viscosity,  $v$  the particle velocity and  $a$  its radius, cannot be used and we need to use various correction factors depending on the distance between the particle and the substrate. For large distances ( $h > 1.04 a$ , where  $h$  is the distance from the center of the particle) Goldman, *et al.*, [21] showed that the Faxen correction factor

$$F = 6\pi\mu av \left( 1 - \frac{9}{16} \frac{a}{h} + \frac{1}{8} \left( \frac{a}{h} \right)^3 - \frac{45}{256} \left( \frac{a}{h} \right)^4 - \frac{1}{16} \left( \frac{a}{h} \right)^5 \right)^{-1} \quad (5)$$

deviates less than 10%. Yang, *et al.*, [22] have used this correction factor for small particles but for the  $2.5 \mu\text{m}$  particle size, that is considered here, this corresponds to a distance of at least 100 nm. Below this distance or when the particle is in contact with the substrate one can use the lubrication values of this correction [23]

$$F = 6\pi\mu av \left( \frac{8}{15} \ln \left( \frac{h-a}{a} \right) - 0.9588 \right) \quad (6)$$

where we assumed the particle not to rotate. Table 1 exemplifies these corrections on a centered,  $5 \mu\text{m}$  particle in water with a viscosity  $\mu = 8.9 \cdot 10^{-4} \text{ Pa}\cdot\text{s}$ . We note here that the hydrodynamic predicted velocities for particles in contact with the substrate are 160 times larger than experimentally observed and presented in the next section. The origin of this discrepancy could be the various surface effects as described by Brevik, *et al.*, [24] or the particle floating at a considerable distance from the substrate. When considering angle or distance variations one needs to take into account the variations of the ratio between the  $p$ - and  $s$ -polarization and the shift between the maximal force and maximal intensity. Indeed, these characteristics of the evanescent force change as the particle is moved or the angle of incidence changed. A more complete microfluidic approach would include the particle angular rotation, its surface roughness [25], the buoyancy force, the optical torque, surface friction and the hydrodynamic lift force.

Table 1. Hydrodynamic velocities calculated using different correction factors

angle	h	Vert. force	Hor. Force	Correction	Velocity
61°	2.51μm	-400pN	600pN	Stokes	14mm/s
				Faxen	4.6mm/s
				Krishnan	3.6mm/s
	5.5μm	-1.0pN	6.0pN	Stokes	143μm/s
				Faxen	107μm/s
				Krishnan	275μm/s
70°	2.51μm	-67pN	45pN	Stokes	1.1mm/s
				Faxen	352μm/s
				Krishnan	275μm/s
	3 μm	-7.5pN	5.1pN	Stokes	121μm/s
				Faxen	91μm/s
				Krishnan	275μm/s

### 3. Experiment

In the following sections, we verify and explore the near-field deflection force on microparticles using a TIR objective. The dependence of this force on particle size and refractive index is experimentally determined and we apply this to passive optical sorting of microparticles in a microfluidic chip.

#### 3.1 Setup

A near-infrared (IPG Photonics, 1070 nm, 5 W) laser beam was sent through the back aperture of a Plan Apo TIR objective lens (Nikon, x100, NA 1.49, oil immersion) of an inverted microscope (Nikon, TE2000-E). This beam was de-magnified to a collimated diameter of 0.4 mm. A beam splitter mounted on a translation stage was placed beneath the objective, allowing the beamlet to be carefully translated to the edge of the back aperture of the objective and obtain evanescent (near-field) illumination at the sample plane [see Fig. 6(a)]. The sample was illuminated with incoherent light through a high-NA condenser, imaged using the TIR objective and captured by a high frame-rate camera.

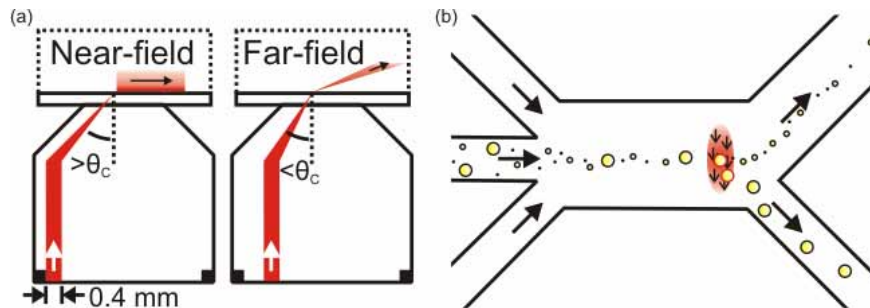


Fig. 6. (a). Near-field and far-field generation through a high-NA TIR objective lens by choice of beamlet position at the back aperture. Light rays within 0.4 mm of the back aperture extremity are incident with the coverslip-sample interface at an angle greater than the critical angle for total-internal reflection  $\theta_c$ , producing evanescent waves (EW). (b) Passive optical sorting of microparticles by size using an evanescent field focused into a microfluidic chip. The sample fluid is hydrodynamically focused to pass over an evanescent focal spot and the size-dependence of the optical deflection force causes larger particles to be guided into a separated flow channel.

### 3.2 Sample chamber

The sample chamber composed of a conventional geometry with two glass coverslips (BK7) separated with a vinyl spacer (thickness 100  $\mu\text{m}$ ). The sample consisted of polystyrene microparticles dispersed in deionized water. The chamber was sealed with nail varnish to prevent leakage and movement of the coverslip.

### 3.3 Microfluidic flow channels

Microfluidic chips were employed to perform optical sorting and fluidic separation of particles by size using this evanescent geometry. Chips were fabricated using standard soft lithography techniques [26] from polydimethylsiloxane (PDMS) and irreversibly sealed to a glass coverslip. This allows the objective to be index-matched and implemented close below the channels, which were designed to hydrodynamically focus the sample solution into a thin stream along the centre of a flow channel. This is, where an evanescent field was positioned using the optical setup outlined above. A cross-type optical chromatography geometry [27] was used, where the optical deflection force is orthogonal to the flow direction, allowing continuous passive sorting of particles with a single optical beam.

## 4. Experimental results and discussions

Experimental observations were made of the behavior of microparticles in the presence of an evanescent field generated by an off-axis beamlet focused by a TIR objective lens. Particle trajectories were plotted using particle tracking software, velocities calculated and the results compared to theoretical predictions. The dependence of the evanescent force on particle diameter and refractive index is explored and we demonstrate how this simple optical setup can be implemented in passive sorting of microparticles by size in a microfluidic chip.

### 4.1 Guiding of microparticles near a surface

Experiments were conducted using a 0.4 mm diameter collimated beamlet, positioned at the outer extremity of the back aperture of a TIR objective lens. This beamlet was focused into a sample chamber, containing 5  $\mu\text{m}$  polystyrene microparticles immersed in deionized water, such that an evanescent wave formed at the glass/water interface between the coverslip and sample solution. The polarizations  $s$  and  $p$  were obtained by rotating a half-wave plate in the beam path immediately before the de-magnifying telescope. A high concentration of microparticles in the sample chamber caused microparticles to continuously traverse along similar paths, outlining the deflective force vectors and position of the evanescent field. The dynamic behavior of the particles in the presence of the evanescent field was captured and tracked using LabView particle tracking software [28] (see Fig. 7). The evanescent guiding of microparticles is such that they are confined to the centre of the plane where the focused beam was located.

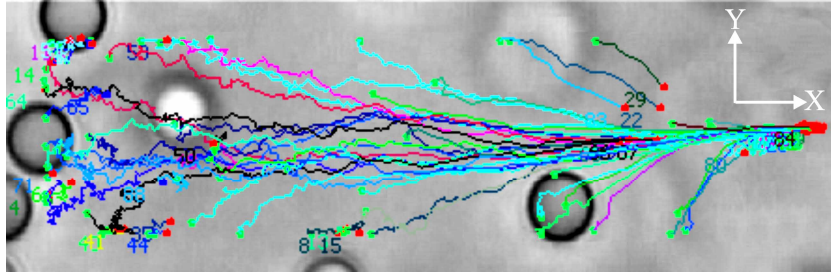


Fig. 7. Particle trajectories overlaid onto a snapshot of a one minute long video of 2  $\mu\text{m}$  polystyrene microparticles in the presence of an evanescent field, generated by a TIR objective lens illuminated by an off-axis beamlet. The initial position of the microparticles is indicated by a green spot, the lines show their path over time and the red spot indicated the point at which the particle is lost by the tracking software. Particles are guided by the evanescent wave in the positive  $x$  direction.

In the presence of the optical field, microparticles were seen to be pulled towards the surface by the strong gradient forces and subsequently guided along the evanescent field due to the deflection forces. The guiding velocity of microparticles was calculated from the tracking data for particles that traversed down the center of the elliptical evanescent spot,  $y=0$ . Mean velocities for multiple particles were then calculated for each  $x$  position, a typical plot of which is shown in Fig. 8(a), which is the power-normalized velocity for 36 different 5  $\mu\text{m}$  polystyrene particles.

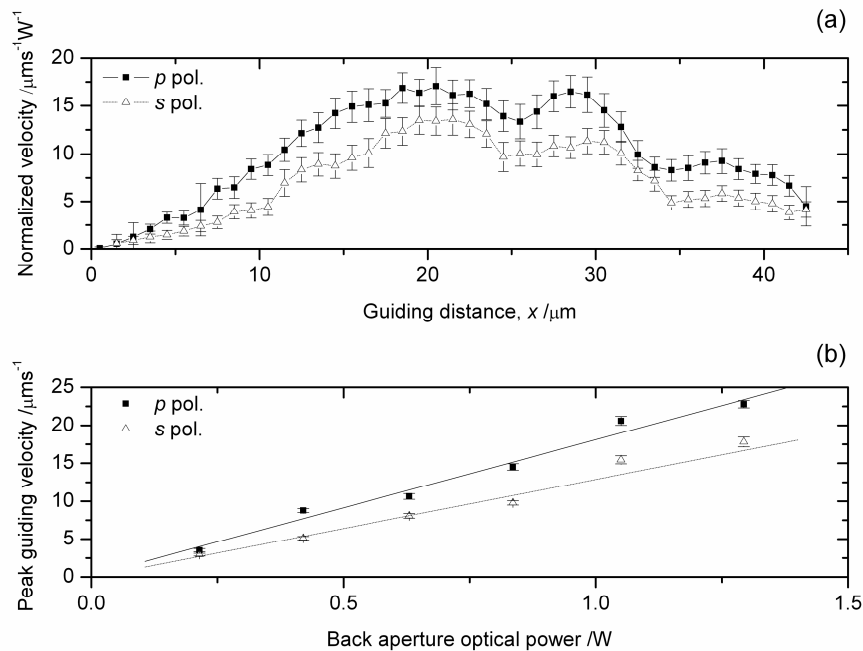


Fig. 8. Velocities of 5  $\mu\text{m}$  polystyrene particles guided by an evanescent field generated using a TIR objective lens, illuminated with  $p$  and  $s$  polarized laser light at the edge of the back aperture. (a) Mean guiding velocity normalized per unit power, as a function of distance traveled along the evanescent field. The  $x$ -axis here corresponds to the  $x$ -axis in Fig. 2. Each data point is the mean velocity of 36 particles (6 particles at 6 different powers) divided by the back aperture optical power, with the associated standard error in the mean. (b) Linear dependence of peak guiding velocity on the optical power at the back aperture of the TIR microscope objective lens. Each data point represents the mean peak velocity of 6 particles and the associated standard error in the mean.

In the region  $x < 0$  the microparticles exhibit Brownian motion until trapped against the surface near  $x = 0$  due to the gradient forces and accelerated in the positive  $x$  direction due to the evanescent field. The most intense region of the evanescent focal spot is at  $x = 21$ . We attribute the non-Gaussian velocity profile seen here to multiple reflections in the coverslip and/or aberrations from the TIR objective lens. The largest guiding velocity observed was for  $5 \mu\text{m}$  particles in  $p$  polarized light, with a back aperture power of  $1.3 \text{ W}$  and was measured to reach  $23 \pm 0.5 \mu\text{ms}^{-1}$ . It should be noted that the velocity can be increased by an order of magnitude by a small translation of the beamlet to increase the propagating component whilst still maintaining a reasonable guiding distance before leaving the surface [see Fig. 3(a)].

After traversing the evanescent field the microparticles were found to be lifted up and subsequently lost by the tracking software. We attribute this to a small fraction of transmitted (far-field) light passing through the glass/water interface due to the angle of incidence [see Fig. 3(a)]. It was found not possible to entirely remove this effect. Due to the illumination of the edge of the back aperture, the focal spot is highly sensitive to diffraction and aberrations, which could give rise to rays propagating below the critical angle for TIR and generate a propagating component in the sample chamber.

The  $p$  polarized evanescent wave is seen to impart a higher guiding force to the particles than  $s$  polarized light. It should be noted that many factors play a role in deciding the dominant polarization state, including sphere size and polarizability, as well as the laser wavelength and incident wave vector [16, 24, 29]. As predicted from our model and from previous work [14, 16], the velocity of the microparticles in the evanescent field increased linearly with incident laser power, as seen from the experimental results in Fig. 8(b). Gradients of  $18.0 \pm 0.4 \mu\text{ms}^{-1}\text{W}^{-1}$  and  $13.0 \pm 0.4 \mu\text{ms}^{-1}\text{W}^{-1}$  were found for  $p$  and  $s$  polarized light respectively, for  $5 \mu\text{m}$  polystyrene spheres in the evanescent field.

Figure 5 also shows that the experimental measurements are in good qualitative agreement with the predictions from the theoretical model. In particular, both, the experiment and the theory, show a shift between the maximum beam intensity and maximal guiding force/velocity. We also observe a similar ratio between the optical forces in  $s$  and  $p$  polarization as predicted theoretically for an incident angle of  $61^\circ$ . Further, the lift of the particle, at the end of its trajectory, can also be understood when considering the simulations for incidence angles very close to the critical angle such as  $60^\circ$ .

The use of a high magnification TIR objective lens in this work produces a higher evanescent field power density (500 times greater than Almaas, *et al.*, [20]) compared to previous works using prism-generated evanescent waves. Guiding velocities are an order of magnitude higher than in the work by Oetama and Walz (prism-generated evanescent waves) for equivalent optical powers, particle size and material (refractive index). Guiding velocities are comparable to studies where particles are guided in the evanescent field of a waveguide, such as Grujic, *et al.*, [13]. The high guiding velocity using a TIR objective facilitates the manipulation of microparticles against a fluid flow and in the next section we apply this near field technique to optical sorting in the presence of flow.

#### 4.2 Passive sorting of microparticles in an evanescent field

Making use of a high magnification TIR objective lens allows a tiny evanescent spot to be produced with a higher optical power density and increased guiding velocity compared to prism-generated TIR techniques. The optical forces are sufficiently large to move particles during fluid flow, allowing evanescent fields to be applied to passive sorting of microparticles according to their intrinsic properties, based on their interaction with the evanescent field. Here, the dependence of the evanescent guiding force on particle size and refractive index for this geometry is characterized, before results on the successful passive sorting of microparticles by size in a microfluidic chip using this technique are presented.

This evanescent sorting technique differs to previous works [12,13] in that it was conducted in a microfluidic chip in the presence of flow, allowing the different particle 'species' to be split into separate fluidic channels using the evanescent field; and that no active switching mechanism is required, making it an entirely passive sorting technique, respectively. It should also be noted that here micron-sized particles were sorted, making it applicable to biological cell sorting. Manipulation of biological cells using the near-field may present advantages due to low penetration depth of the electromagnetic field, reducing the risk of photodamage to the cell, a common point of concern with optical manipulation techniques.

As the guiding velocity is proportional to the induced evanescent force on particles in the optical field, a comparison of guiding velocities for a range of particle sizes and refractive indices provides a good indication of the sensitivity of this geometry for optical sorting. The guiding of polystyrene and silica particles, of refractive index of 1.59 and 1.37 respectively, was recorded for sphere diameters of 1, 3 and 5  $\mu\text{m}$ . The peak guiding velocities were calculated and are plotted in Fig. 9(a), for a fixed back aperture optical power of 1.05 W. The guiding velocity of polystyrene spheres is on average  $2.9 \pm 0.7$  greater than silica spheres of the same diameter. The peak guiding velocity increases by  $3.0 \pm 0.5 \mu\text{ms}^{-1}$  per  $\mu\text{m}$  increase in diameter for polystyrene spheres and  $0.7 \pm 0.2 \mu\text{ms}^{-1}$  per  $\mu\text{m}$  for silica, over this size range. Size dependence is expected, since as the particle size increases, the area of overlap between the particle and the evanescent field increases, which results in a stronger radiation force being exerted on the particle [15]. For the size range considered here, our model predicts the optical force to scale linearly with the particle diameter (see Fig. 5).

To harness the size-dependence of the evanescent force for particle sorting, a cross-type optical chromatography geometry [27] was employed. Unlike the sorting geometry used by Hart and Terray [30] where particles are separated to points of equilibrium between the opposing optical scattering and fluid flow Stokes force, our beam provides an optical force orthogonal to the direction of fluid flow. This is desirable as particles can be continuously separated whilst remaining in continuous flow, allowing different species to be passively flowed into separated fluid channels downstream in the chip. This near-field sorting geometry is characterized in Fig. 9(b) for polystyrene spheres of 1  $\mu\text{m}$  to 5  $\mu\text{m}$  in diameter.

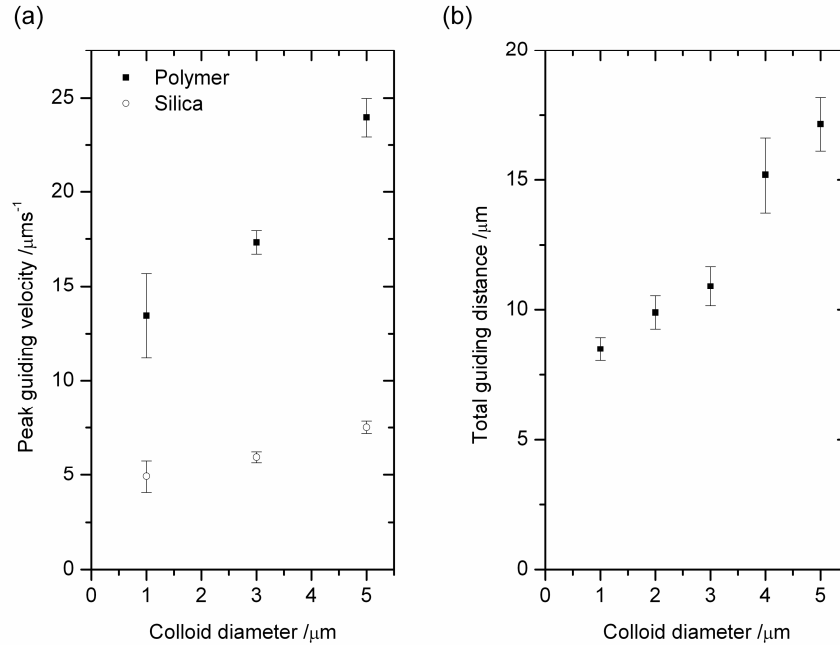


Fig. 9. Size and refractive index discrimination of microparticles in an evanescent field generated using a TIR objective lens. (a) Dependence of guiding velocity on particle diameter for refractive indices 1.59 and 1.37, namely polystyrene and silica respectively, for a power of 1.05 W at the back aperture. (b) Separation of microparticles in a  $20 \mu\text{ms}^{-1}$  fluid flow using an optical power of 1.3 W at the back aperture. The guiding distance is that traveled by a particle entering the evanescent field at a pre-defined position, traveling some distance orthogonal to fluid flow due to the optical field, before leaving the field with the bulk fluid flow. Data points are the mean distance traveled for a minimum of 5 particles that enter the field within  $\pm 2 \mu\text{m}$  of a pre-determined position of maximum evanescent guiding velocity.

The characterization was conducted in a sample chamber, using a motorized microscope stage that translated the sample across the beam at  $20 \mu\text{ms}^{-1}$ . The particles entered the field, orthogonal to the evanescent guiding direction, at the pre-determined point in the evanescent field that provides the largest evanescent guiding force [ $x = 21 \mu\text{m}$ , Fig. 8(a)]. As the particles flowed into the field, they were perturbed some distance in a direction orthogonal to the flow direction, which is dependent on the particle diameter, optical power and flow speed. Fig. 9(b) shows a linear dependence of the guiding distance on the size of particles, whilst in a fluid flow. For this size range of particles, the guiding distance was found to increase by  $2.0 \pm 0.2 \mu\text{m}$  per unit  $\mu\text{m}$  increase in particle diameter, for polystyrene particles passing through the evanescent field at  $20 \mu\text{ms}^{-1}$  and with 1.3 W back aperture optical power.

The sorting capability of this technique was taken a step further and realized on a polydisperse mixture of 1, 3 and  $5 \mu\text{m}$  polystyrene spheres within a PDMS microfluidic chip. The chip hydrodynamically focussed the sample solution into a narrow laminar stream, which subsequently passed through an evanescent field [see Fig. 6(b)]. The dimensions of the input channels were  $50 \mu\text{m}$ -wide, the central sorting channel was  $150 \mu\text{m}$ -wide,  $300 \mu\text{m}$ -long and the two output channels widths were mismatched, such that all microparticles passed into a wider  $100 \mu\text{m}$ -wide channel unless optically-deflected into a narrower  $50 \mu\text{m}$ -wide channel by the evanescent field. The heights of the channels were  $70 \mu\text{m}$  throughout. The spheres typically flowed along the bottom of the channel due to the density difference between the microparticles and the surrounding medium, allowing them to interact with the evanescent field on the base of the channel. Flow rates were controlled via an external syringe pump and were typically  $50 \mu\text{ms}^{-1}$  in the channel containing the evanescent field.

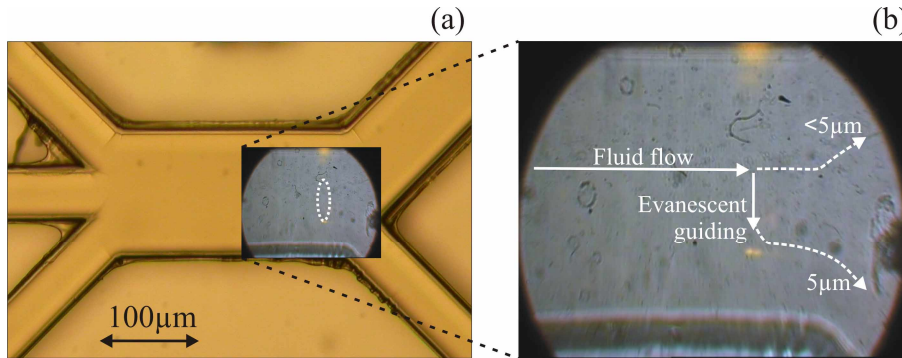


Fig. 10. Passive sorting by particle size in a microfluidic chip using evanescent waves. (a) Chip design to hydrodynamically focus sample through evanescent field focal spot. Approximate focal spot position is indicated by the dashed white ellipse. (b) Supplementary real time video of the sorting of 5  $\mu\text{m}$  polystyrene spheres from a polydisperse mixture of 1, 3 and 5  $\mu\text{m}$  spheres.

The evanescent field ( $\sim 1$  W at the back aperture) was sufficient in deflecting 5  $\mu\text{m}$  particles up to 20  $\mu\text{m}$  (in a direction orthogonal to the flow) from the main particle stream, thus allowing them to exit via the smaller output channel of the chip (see supplementary video). The smaller 1 and 3  $\mu\text{m}$  particles were barely deflected and exited the chip via the larger output channel staying within the laminar stream. An increase in flow rate, optical power and particle density could potentially increase the throughput of sorting from the order of one particle per second, shown in this footage, to tens or hundreds of particles per second.

## 5. Conclusion

By illuminating a TIR objective with an off-axis beamlet, the deflection of microparticles using near-field laser light has been demonstrated. In our new geometry, evanescent fields were created by positioning a beamlet of 0.4 mm diameter at the edge of the back aperture of this high-NA objective lens. By carefully translating such a beamlet across the back aperture from the centre to the edge, the optical field at the sample plane can be changed from the far-field to the near-field regime.

A fully vectorial finite element method for this geometry is presented. The optical force profile predictions for the evanescent field were found to agree qualitatively with experimental observations. In this new geometry,  $p$  polarized light was found to induce a greater guiding force on the microparticles than  $s$  polarized light and that the maximum force is shifted with respect to the beamlet intensity maxima.

Experimentally, the maximum guiding velocity due to the evanescent force was found to increase by  $3.0 \pm 0.5 \mu\text{m s}^{-1}$  per  $\mu\text{m}$  increase in diameter for polystyrene spheres and  $0.7 \pm 0.2 \mu\text{m s}^{-1}$  per  $\mu\text{m}$  for silica over the diameter range of 1  $\mu\text{m}$  to 5  $\mu\text{m}$ . This was employed for optical sorting of microparticles in a microfluidic chip. By exploiting the linear dependence of the evanescent guiding force on particle size, entirely passive sorting of 5  $\mu\text{m}$  spheres from a polydisperse mixture of 1  $\mu\text{m}$ , 3  $\mu\text{m}$  and 5  $\mu\text{m}$  polystyrene spheres was characterized and accomplished. This method may readily be extended to initiate large area optical sorting within microfluidic devices and the potential for decoupling the light field that initiates the sorting from the observation optics (which could be implemented from above).

## Acknowledgments

This work was supported by funds from the UK Engineering and Physical Sciences Research Council.